Phys. Status Solidi A **206**, No. 8, 1885–1891 (2009) / **DOI** 10.1002/pssa.200881460

physica status solidi pss a
www.pss-a.com
applications and materials science

Dislocation nucleation from surface step in silicon: The glide set versus the shuffle set

Julien Godet*, **Pierre Hirel, Sandrine Brochard, and Laurent Pizzagalli**

PhyMat, UMR 6630, Université de Poitiers, CNRS, SP2MI, BP 30179, 86962 Chasseneuil, Futuroscope Cedex, France

Received 17 September 2008, revised 26 March 2009, accepted 31 May 2009
Published online 20 July 2009

PACS 02.70.ns, 62.20.F−, 61.72.uf, 61.72.Lk, 62.25.−g

* Corresponding author: e-mail julien.godet@univ-poitiers.fr, Phone: +33 549496558, Fax: +33 549496692

We have studied the mechanisms of dislocation nucleation from surface defects in silicon submitted to various stresses and temperatures. Molecular dynamics simulations with three classical potentials have shown the existence of two different plastic modes in silicon which can be activated from surfaces. At high temperatures and low stresses dislocations nucleation occurs in the {111} glide set planes, while at low temperatures and large stresses it occurs in the {111} shuffle set planes. The analysis of dislocation cores and kinks shows structures like those well known in bulk silicon. This study supports the idea that plasticity in crystalline Si structures could be governed by dislocation nucleation from surfaces.

© 2009 WILEY-VCH Verlag GmbH & Co. KGaA, Weinheim

1 Introduction The plasticity of silicon is not fully understood despite the huge amount of studies done for several decades. This is partly due to the fact that the cubic diamond structure of Si is composed of two interwoven fcc lattices, giving rise to two sets of {111} slip planes, the "shuffle" and the "glide" [1] (Fig. 1). Originally, the dislocation was thought to slip in the shuffle set plane because only one Si–Si bond had to be broken instead of three in the glide set plane. However, in the ductile regime at high temperature, only dissociated dislocations in the glide set planes are observed [2]. Since the works of Rabier et al. [3, 4] where silicon is deformed in the brittle regime, i.e., at low temperature, but under very high confining pressure to avoid cracks formation, perfect dislocations belonging to the shuffle set planes have been identified. These observations support the existence of two plastic regimes, the glide and the shuffle [5, 6]. The relevant questions are: how can we pass from one regime to the other and what is the role of mobility and nucleation of dislocations in the transition. In nanostructures or in perfect silicon crystals without mechanisms such as Frank–Read to multiply dislocations, surface irregularities have been proposed as sources of dislocations nucleation [7–10]. Several atomistic simulations have already shown the possibility to nucleate dislocations from surface defects in Al [11, 12] and in Si [13, 14]. However, in silicon, the simulations have only shown the dislocations nucleation in the shuffle set plane under low temperature and high stress conditions. The scope of this paper is to show the possibility of nucleating dislocation from surfaces in the glide set planes as well as in the shuffle set planes, and to define the stress–temperature conditions for both plastic regimes in silicon, which is critically lacking for a better understanding of silicon plasticity.

In this paper, we carried out molecular dynamics simulations to study dislocation nucleation from silicon surface steps submitted to a large range of temperatures and stresses. After a short presentation of the methods and models, we describe the results obtained with three classical potentials. They show the formation of dislocation loops either located in the shuffle set planes or in the glide set planes only depending on stress magnitude and temperature. We analyze the dislocation cores and kinks formed from surfaces, and compare them to the existing one in bulk silicon. Finally, we conclude that dislocation nucleation from surfaces is a key mechanism for governing silicon plasticity in systems such as nanostructures.

WILEY InterScience DISCOVER SOMETHING GREAT

© 2009 WILEY-VCH Verlag GmbH & Co. KGaA, Weinheim

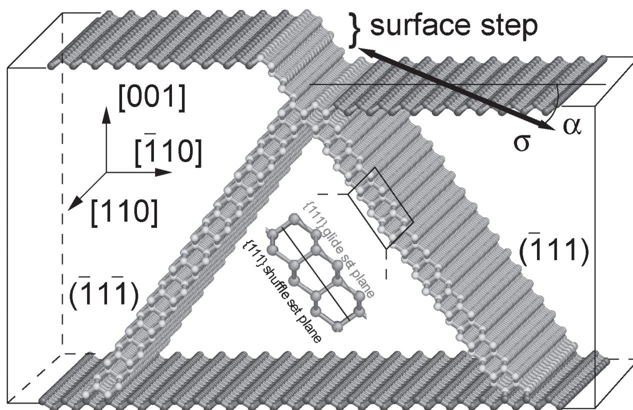

Figure 1 (online color at: www.pss-a.com) Atomic system modeling a ledge on the (001) silicon surface. Only atoms on the surfaces (dark gray) and inside both slip planes ($\bar{1}1\bar{1}$) and ($\bar{1}11$) (light gray) are represented [16]. The uniaxial stress σ inside the (001) plane forms an angle α with respect to the [$\bar{1}10$] direction.

2 Simulations setup

2.1 Models We considered a slab of silicon including several half atomic layers on its surface forming a ledge with a {111} face (Fig. 1). Both bottom and upper surfaces are free and $p(2 \times 1)$ reconstructed [15]. Periodic boundary conditions have been used along the step line, and we kept frozen both {$\bar{1}10$} surfaces in the last direction for maintaining the applied stress. The atomic system contains around 40 000 atoms, but bigger systems up to 150 000 atoms have been also tested without significant differences.

2.2 Computational methods We considered three interatomic potentials to describe the Si–Si interaction: the potential of Stillinger and Weber (SW) [17], based on a linear combination of two- and three-body terms, the Tersoff potential [18] including many-body interactions; thanks to a bond order term in the functional form, and the environment-dependent interatomic potential [19] (EDIP) designed specifically to compute defect structure properties. To get the plastic relaxation processes, we carried out molecular dynamics simulations on a time scale ranging from 50 to 400 ps, with a time step of 0.5 fs. The temperature was set between 0 and 1500 K, and controlled by velocity rescaling.

2.3 Technique for stress application To simulate the effect of an applied uniaxial stress σ (Fig. 1), we deformed the system following the strains calculated using the silicon compliances S_{ijkl} [1]. S_{ijkl} are obtained from the elastic constants C_{ijkl}, computed for each potential used. In this work, the uniaxial stress is contained into the (001) plane, but its direction can be disorientated with an angle α with respect to the [$\bar{1}10$] direction (Fig. 1).

3 Results

Experimentally, the plasticity of bulk silicon is known to operate in two distinct regions of the stress–temperature diagram. At high temperature and low stress, dislocations are dissociated and slip in the glide set plane, while at low temperature and high stress, they are perfect and located in the shuffle set plane. To study the occurrence of plasticity from surfaces in both regimes, we performed molecular dynamics simulations in the conditions close to those investigated experimentally. In the following, we described the representative results obtained by the three classical potentials, in both relevant regions of the stress–temperature diagram.

3.1 SW potential

3.1.1 Tensile stress The plastic behavior has been investigated by considering different stresses and temperatures. Here, we present molecular dynamics simulations realized for the stress orientation $\alpha = 18^\circ$ giving a resolved shear stress inside the {111} slip planes approximately equivalent for the 90° partial and the 60° perfect dislocations [20].

Low temperature–large stress In this case, we described the simulation at 600 K, for a strain of 13.2%. After few pico seconds, the tensile stress is relaxed by the nucleation of a perfect dislocation loop in the ($\bar{1}11$) shuffle set plane (Fig. 1), increasing the step height (Fig. 2a). A short damping of the atomic structure has been done to remove the thermal agitation and to keep the dislocation on site. The dislocation is characterized by a burgers vector $\boldsymbol{b} = 1/2[01\bar{1}]$, and forms a half loop emerging at the (001) free surface in points A and E. The half loop is composed of two 60° dislocation segments AB and BC and two screw segments CD and DE separated by a kink [21] in D (Fig. 2a). The core structure of the perfect 60° dislocation includes a threefold coordinated atom as already observed in *ab initio* calculations [13]. The screw segment is mainly found in one of its stable configurations given by the SW potential and named "A" in previous works [22, 23]. We note that Fig. 2 is a snapshot of molecular dynamics simulation, and depicts the dislocation configuration during its propagation in presence of a thermal agitation, and does not correspond to the equilibrium position of the dislocation.

High temperature–low stress We then performed simulations at lower stress, about 8.4%, and higher temperature of 1350 K. After 200 ps, a partial dislocation embryo characterized by a Burgers vector $\boldsymbol{b} = 1/6[\bar{1}1\bar{2}]$, appears in a {111} glide set plane. This dislocation moves by the formation and migration of kink pairs and tends to be aligned along the ⟨110⟩ Peierls valleys of silicon as bulk dislocation (Fig. 2b). The half loop connects to the surface step in points A and E and is composed of two 30° dislocation segments, AB and DE, and one 90° dislocation segment BD (Fig. 2b). We easily identify the double period reconstruction of the 30° dislocation on the AB part, as already calculated by classical potentials [24] and tight binding methods [25]. The 90° dislocation is slightly more complex with a double period reconstruction [26] on BC and an asymmetric simple period

© 2009 WILEY-VCH Verlag GmbH & Co. KGaA, Weinheim

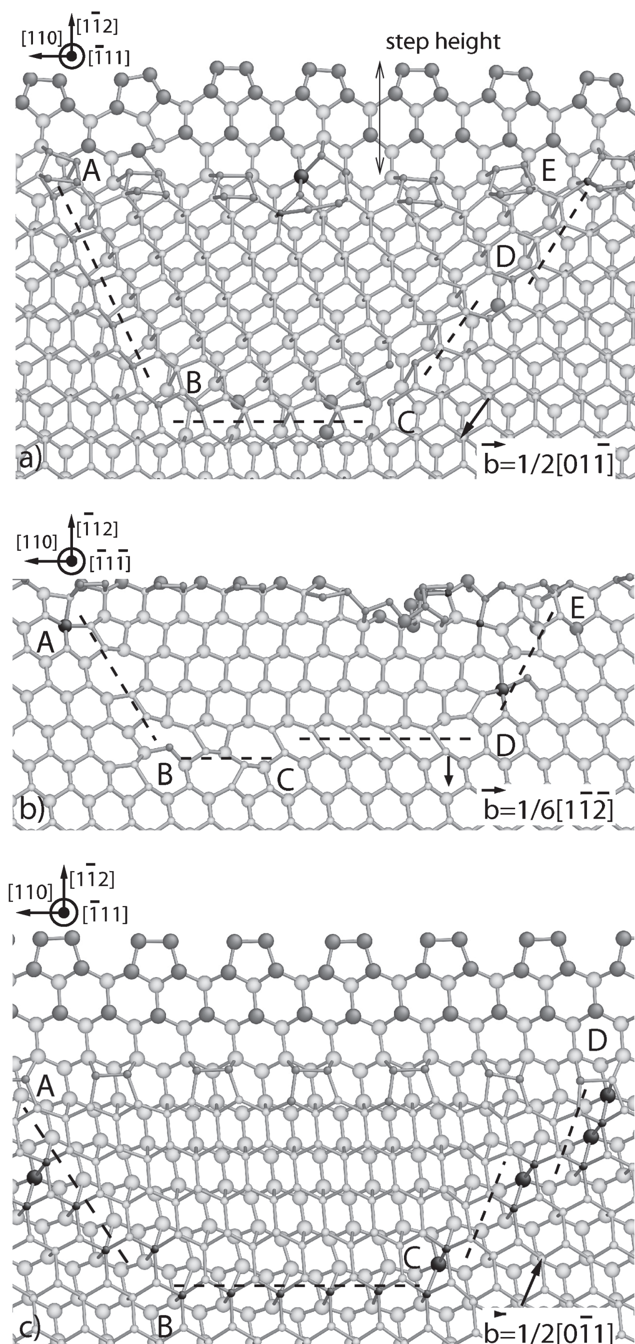

Figure 2 (online color at: www.pss-a.com) SW potential: Atomic configurations of dislocations nucleated in different {111} slip planes. The dashed line is a guide to the eyes emphasizing the dislocation position. The Si atoms located below (above) the slip plane are represented by large (small) balls. The green, light gray, and black balls correspond to three-, four-, and fivefold coordinated Si atoms, respectively [16]. Bonds are drawn according to the distance criterion. (a) and (c) Perfect dislocations nucleated in the ($\bar{1}$11) shuffle set plane at low temperature and large (a) tensile stress or (c) compressive stress. (b) Partial dislocation nucleated in the ($\bar{1}$1$\bar{1}$) glide set plane at high temperature and low tensile stress.

reconstruction [27] on *CD* connected by a partial kink [28] in *C*. We note that the asymmetric simple period reconstruction usually unstable with the SW potential is made possible by the disorientated applied stress.

3.1.2 Compressive stress Two different plastic regimes have been obtained in traction according to the temperature and stress magnitude. To confirm these results we performed simulations on the same system but under compressive stresses. Here, we describe the simulation performed with a stress orientation $\alpha = 45^\circ$ favoring three dislocations: the perfect 60° and screw dislocations, and the 30° partial [20].

Low temperature–large stress At 600 K and −11.2%, we observed the nucleation of a perfect dislocation loop in the ($\bar{1}$11) shuffle set plane crossing the surface step (Fig. 2c). The nucleated dislocation has a Burgers vector $\boldsymbol{b} = 1/2[0\bar{1}1]$, and is mainly lying along the ⟨110⟩ Peierls valley of silicon giving rise to *AB* and *BC* 60° segments and one *CD* screw segment (Fig. 2c). The dislocation core structure is similar to the one in Fig. 2a, but the core atoms are fivefold coordinated probably due to the large compressive stress which brings the atoms closer.

High temperature–low stress For higher temperature (1200 K) and lower stress (−6.3%), instead of partial dislocation, we observed the nucleation of a linear defect from the surface. However, it is not physical and corresponds to an artifact of the SW potential [29].

3.2 Tersoff potential A similar study has then been done with the Tersoff potential in the different regions of the stress–temperature diagram.

3.2.1 Tensile stress

Low temperature–large stress Molecular dynamics have been performed from 0 to 1300 K for stresses up to 20%. Despite the stress orientation $\alpha = 22.5^\circ$ which gives the highest resolved shear stress on the perfect 60° dislocation [20], no dislocation is nucleated. Instead for highest temperature, we only observed an increasing number of fourfold coordinated point defects in silicon [30], leading to the melting of the surface in the vicinity of the step.

High temperature–low stress Here, we chose a stress direction normal to the step line to maximize the resolved shear stress on the 90° partial dislocations [20]. At 1500 K and 10.9%, a partial dislocation is nucleated in a ($\bar{1}$1$\bar{1}$) glide set plane (Fig. 3a), releasing a part of the applied stress by decreasing the step height. The dislocation half loop has a Burgers vector $\boldsymbol{b} = 1/2[1\bar{1}\bar{2}]$, and is connected to the surface in points *A* and *G*. It is composed of two 30° dislocations, *AB* and *FG*, and one 90° dislocation, *BF*, with a double period reconstructed core. The 90° partial includes several kinks, two full [28] in *C* and *E*, and one partial [28] in *D*. We can remark an anti-phase defect [31, 32] inside the kink *C*.

3.2.2 Compressive stress Here, the stress orientation $\alpha = 36^\circ$ has been considered to produce large

© 2009 WILEY-VCH Verlag GmbH & Co. KGaA, Weinheim

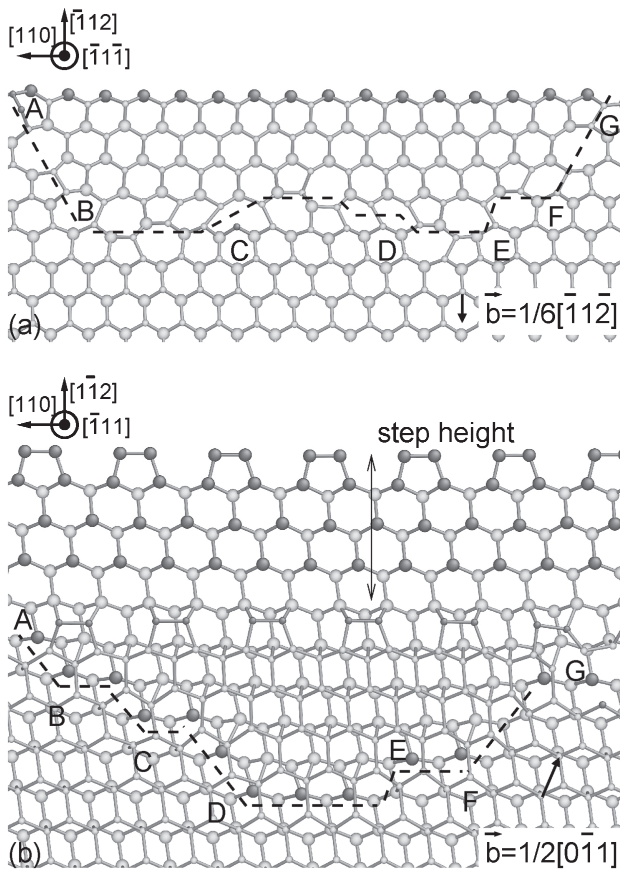

Figure 3 (online color at: www.pss-a.com) Tersoff potential: (a) Partial dislocation nucleated in the ($\bar{1}1\bar{1}$) glide set plane at high temperature and low tensile stress. (b) Perfect dislocations nucleated in the ($\bar{1}11$) shuffle set plane at low temperature and large compressive stress (see legend in Fig. 2).

resolved shear stresses on 30° partial and on 60° perfect dislocations.

Low temperature–large stress For a strain about −11.2%, plasticity occurred when temperature reached 900 K. A perfect dislocation half loop with a Burgers vector $\boldsymbol{b} = 1/2[0\bar{1}1]$ is nucleated from the surface step and glides in a ($\bar{1}11$) shuffle set plane. The dislocation nucleation is accompanied by a decrease of the step height to relax the applied stress (Fig. 3b). *AD* and *DF* segments correspond to two 60° perfect dislocations lying along the ⟨110⟩ directions and include several full kinks in *B*, *C*, and *E*. The dislocation cores include threefold coordinated atoms. The last segment *FG* is a perfect screw dislocation in the "A" configuration [22, 23].

High temperature–low stress Among the different simulations realized in various stress and temperature conditions, no dislocation has been observed in this regime for compressive stress. We only noted surface melting for the highest temperatures.

3.3 EDIP

Although both modes of plasticity have been obtained with two different classical potentials, we carried out simulations with a third classical potential, EDIP, to confirm this result.

3.3.1 Tensile stress

Low temperature–large stress At 300 K, plastic deformations appear for a strain around 13.4% when the stress orientation was set to 18°. We observed the formation of a perfect half loop dislocation with a Burgers vector $\boldsymbol{b} = 1/2[01\bar{1}]$. The dislocation is composed of two 60° segments, *AB* and *BC*, and one screw segment, *CD* (Fig. 4a). Along *AB*, the dislocation core is characterized by fivefold coordinated atoms including some point defects due to the thermal agitation. However, another core configuration is found on *BC* where fivefold coordinated atoms on the upper layer are accompanied by Si–Si broken bonds in the lower plane. More investigations are needed for a better characterization. The screw dislocation is found with a core in the "A" configuration [22, 23].

High temperature–low stress Despite several stress orientations no partial dislocation has been formed. Instead, we observed surface melting from temperature around 1200 K.

3.3.2 Compressive stress

Low temperature–large stress For a compressive strain about −7.4% with $\alpha = 22.5°$ and a temperature of 300 K, we observed an artificial large shear strain of the overall shuffle set plane crossing the step, before a perfect dislocation half loop with a Burgers vector $\boldsymbol{b} = 1/2[0\bar{1}1]$ occurs in the same plane (Fig. 4b). This shear strain is a well-known spurious behavior of EDIP when simulations are performed in compression [20]. The dislocation lies along the ⟨110⟩ directions with two parallel screw segments, *AB* and *EF*, and two 60° segments, *BC* and *CE*. The latter segment includes a full kink in *D*. The screw dislocation, *EF*, is mainly found in the "A" configuration while the other screw segment, *AB*, is close to the "B" configuration previously calculated [22, 23]. We recall that figures are snapshots from molecular dynamics simulations and do not reflect the structure stability. The cores of the 60° dislocations include fivefold coordinated atoms.

High temperature–low stress The simulation performed with EDIP at 1300 K and −6.3% for a stress direction $\alpha = 45°$, leads to a pre-melting of the surface followed by the nucleation of a partial half loop dislocation in a glide set plane (Fig. 4c). The dislocation emerges from the surface step and is characterized by a Burgers vector $\boldsymbol{b} = 1/2[\bar{1}\bar{2}1]$. It is composed of one 90° segment, *AB*, with a simple period reconstruction, and two 30° segments, *BC* and *CE*, with a double period reconstruction, including a migration kink in *D* as described earlier [28].

4 Discussion

In this work, we mainly focused on the onset of plasticity under high stress–low temperature or low stress–high temperature conditions, where dislocations have been experimentally observed in bulk silicon. However, we extended our investigations to the overall stress–temperature diagram to probe the mechanical

© 2009 WILEY-VCH Verlag GmbH & Co. KGaA, Weinheim

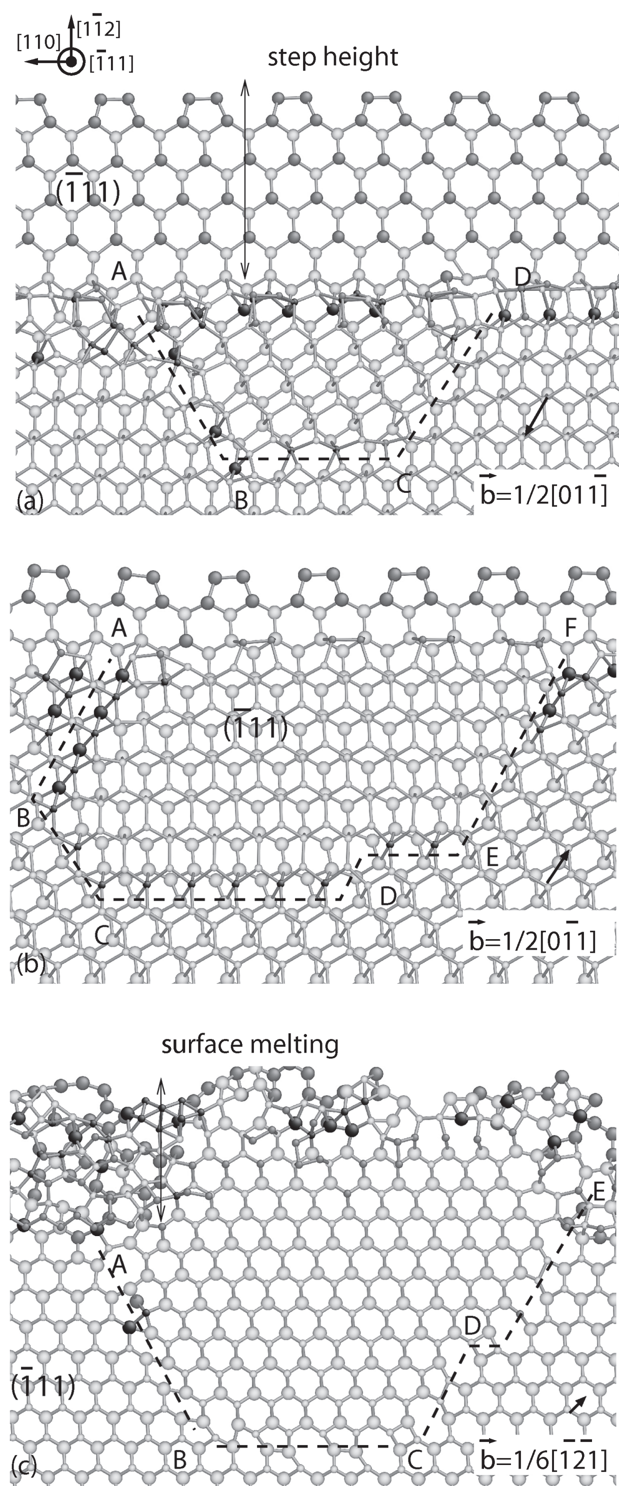

Figure 4 (online color at: www.pss-a.com) EDIP: (a) and (b) Perfect dislocations nucleated in the ($\bar{1}$11) shuffle set plane at low temperature and large (a) tensile stress or (b) compressive stress. (c) Partial dislocation nucleated in the ($\bar{1}$11) glide set plane at high temperature and low compressive stress (see legend in Fig. 2).

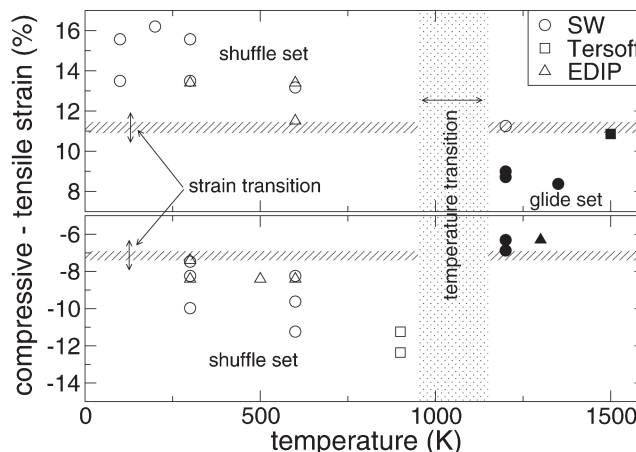

Figure 5 Strain–temperature diagram resuming the simulation conditions where dislocations have been nucleated. The figure sums up the results obtained for the three interatomic potentials and for various stress orientations. The full (empty) symbols correspond to dislocations nucleated in the glide (shuffle) set planes.

behavior of the silicon surface under a larger range of external conditions. For each stress magnitude considered, the structure is firstly relaxed at 0 K. Then during the molecular dynamics simulation, the temperature is increased by steps until the first plastic event appears. The results obtained with the three interatomic potentials are summarized in the strain–temperature diagram (Fig. 5). As expected from bulk plasticity knowledge, the results clearly define two distinct regions corresponding to two kinds of plastic events nucleated from surfaces. At high strain ($<-6\%$ in compression and $>11\%$ in tension) and low temperature (≤ 900 K) the dislocations are nucleated in the shuffle set, while at low strain (between -6 and 11%) and high temperature (≥ 1200 K) the dislocations are nucleated in the glide set.

Both plastic regions are separated by temperature and strain transition areas represented by dotted and dashed areas in Fig. 5. The simulations performed in these transition areas mainly lead to complex atomic rearrangements without the occurrence of glissile events. For example, the simulation realized at 1200 K and 11.2% leads to the formation of a dislocation in the shuffle set despite the high temperature applied. However, this dislocation only slips on few Burgers vector before it is transformed into a large rearrangement of the atomic structure. The case with high temperature and large stresses has also been investigated by directly imposing high temperature on largely stressed system. However, fractures or melting occur before plastic events, which is out of scope of this study.

4.1 Comparison of silicon plasticity occurring in bulk and from surfaces Experimentally, the ductile regime of bulk silicon where plasticity occurs in the glide set planes, has been observed from 600 up to 1400 K [37], while the experiment under high confining pressure has only been realized at room temperature [38]. Here the shuffle–glide transition temperature for the nucleation of

© 2009 WILEY-VCH Verlag GmbH & Co. KGaA, Weinheim

dislocation from surfaces can be roughly estimated between 900 and 1200 K. Despite the missing information about the transition temperature from both theory and experiment, overall the transition temperature appears in relatively good agreement when plasticity occurs in bulk or from surfaces. Note that higher temperatures in simulations can be explained by small time scales compared to experiments.

In our simulations, plastic events only occur for relatively high strains from 6 to 13%, compared to the usual stresses observed experimentally in bulk silicon. This is partly due to the different processes generating dislocations in both cases. In bulk, dislocations are multiplied by mechanisms such as Frank–Read at quite low stresses [33], while in systems such as nanostructures, where Frank–Read mechanisms are prevented by small dimensions, dislocations are formed from surfaces at relatively high stresses in order to compensate the image force on the dislocation due to the surface. Such magnitude of stresses are relatively common in perfect nanostructures [13, 34–36] and still remain lower than the theoretical yield stress of Si [20].

Our results also support the idea that bulk dislocations observed in the glide set are directly nucleated in the glide set plane, while those observed in the shuffle set are in the same way nucleated in the shuffle set. No cross slip from glide to shuffle set plane (and *vice versa*) has been observed in our simulations. In the previous work, the mobility of dislocations in the glide set and in the shuffle set has been discussed [6]. The authors conclude that dislocations in the shuffle set are always more mobile than dislocations in the glide set on the full range of temperature and stress. Here, our results clearly show that dislocation nucleation from the surface can be activated in both sets of $\{111\}$ plane. Consequently the dislocation nucleation appears more dominant than the dislocation mobility to govern the onset of plasticity in silicon.

4.2 Stress dependence Although very large stresses are required to nucleate dislocations from surfaces in silicon, the nucleation is relatively sensitive to the stress orientation used in the simulation. In this study, we focused on the results obtained for stress orientations which have the advantage to produce similar resolved shear stress on partial and perfect dislocations. In particular, the stress orientation $\alpha = 18^\circ$ in traction and $\alpha = 36–45^\circ$ in compression. For both cases, we observed two types of dislocations according to the stress magnitude and temperature used. The activation of plasticity inside the glide set or the shuffle set planes is then independent of the stress orientation.

We noted the elastic limit smaller in compression than in traction is a common feature of the anharmonic potential well of silicon atoms. This difference does not prevent the occurrence of both plastic regimes, but the transition appears at smaller stresses in compression than in traction.

4.3 Potential dependence The simulations based on three different interatomic classical potentials lead to qualitatively equivalent results. Although all potentials present spurious behaviors preventing dislocation nucleation in some conditions, for each of them we observed a transition in silicon plasticity depending on the applied stress and temperature. We note a higher transition temperature for the Tersoff potential around 1500 K compared to 1200–1350 K for others. This fact can be explained by the much higher melting point of the Tersoff potential around 3000 K compared to 1500 K for the others.

Overall molecular dynamics simulations gave rise to similar core structures and reconstructions for all classical potentials. However, we note differences in the shape of dislocations. This can be explained by differences in structure stability and migration energies given by the three classical potentials [23, 28] which are known to play on the dislocation dynamics [28].

5 Conclusion Through numerous molecular dynamics simulations based on three classical potentials for silicon, we brought new arguments confirming that two plastic regimes can be solely activated from silicon surfaces. One occurs at high temperature and low stress in the $\{111\}$ glide set planes by the formation and the propagation of partial dislocations. The other appears at low temperature and very large stress in the $\{111\}$ shuffle set planes, and is characterized by the nucleation and the propagation of perfect dislocations. Such plastic mechanisms from surfaces are currently obtained in the vicinity of crack fronts [8, 9] or in strained nanodesigned materials [35, 36] and could govern the origin of plasticity in a large number of silicon systems.

References

[1] J. P. Hirth and J. Lothe, Theory of Dislocations, second edition (Wiley, New York, 1982).
[2] I. L. F. Ray and D. J. H. Cockayne, Philos. Mag. **22**, 853 (1970).
[3] J. Rabier, P. Cordier, T. Tondellier, J. L. Demenet, and H. Garem, J. Phys.: Condens. Matter **12**(49), 10059 (2000).
[4] J. Rabier and J. L. Demenet, Scr. Mater. **45**, 1259 (2001).
[5] M. S. Duesbery and B. Joós, Philos. Mag. Lett. **74**(4), 253 (1996).
[6] L. Pizzagalli and P. Beauchamp, Philos. Mag. Lett. **88**(6), 421 (2008).
[7] X. J. Ning and N. Huvey, Philos. Mag. Lett. **74**(4), 241 (1996).
[8] G. Xu, A. S. Argon, and M. Ortiz, Philos. Mag. A **75**(2), 341 (1997).
[9] B. J. Gally and A. S. Argon, Philos. Mag. A **81**(3), 699 (2001).
[10] A. S. Argon and B. J. Gally, Scr. Mater. **45**, 1287 (2001).
[11] S. Brochard, P. Beauchamp, and J. Grilhé, Philos. Mag. A **80**(3), 503 (2000).
[12] P. Hirel, S. Brochard, L. Pizzagalli, and P. Beauchamp, Scr. Mater. **57**, 1141 (2007).
[13] J. Godet, S. Brochard, L. Pizzagalli, P. Beauchamp, and J. M. Soler, Phys. Rev. B **73**, 092105 (2006).
[14] S. Izumi and S. Yip, J. Appl. Phys. **104**, 033513 (2008).
[15] D. J. Chadi, Phys. Rev. Lett. **43**(1), 43 (1979).
[16] J. Li, Modell. Simul. Mater. Sci. Eng. **11**, 173 (2003).

© 2009 WILEY-VCH Verlag GmbH & Co. KGaA, Weinheim

[17] F. H. Stillinger and T. A. Weber, Phys. Rev. B **31**(8), 5262 (1985).
[18] J. Tersoff, Phys. Rev. B **39**(8), 5566 (1989).
[19] M. Z. Bazant, E. Kaxiras, and J. F. Justo, Phys. Rev. B **56**(14), 8542 (1997).
[20] J. Godet, S. Brochard, L. Pizzagalli, and P. Beauchamp, Phys. Rev. B **70**(5), 54109 (2004).
[21] L. Pizzagalli, A. Pedersen, A. Arnaldsson, H. Jónsson, and P. Beauchamp, Phys. Rev. B **77**, 064106 (2008).
[22] H. Koizumi, Y. Kamimura, and T. Suzuki, Philos. Mag. A **80**(3), 609 (2000).
[23] L. Pizzagalli, P. Beauchamp, and J. Rabier, Philos. Mag. **83**(10), 1191 (2003).
[24] M. S. Duesbery, B. Joos, and D. J. Michel, Phys. Rev. B **43**(6), 5143 (1991).
[25] R. W. Nunes, J. Bennetto, and D. Vanderbilt, Phys. Rev. B **57**, 10388 (1998).
[26] J. Bennetto, R. W. Nunes, and D. Vanderbilt, Phys. Rev. Lett. **79**(2), 245 (1997).
[27] J. R. K. Bigger, D. A. McInnes, A. P. Sutton, M. C. Payne, I. Stich, R. D. King-Smith, D. M. Bird, and L. J. Clarke, Phys. Rev. Lett. **69**(15), 2224 (1992).
[28] V. V. Bulatov, J. F. Justo, W. Cai, S. Yip, A. S. Argon, T. Lenosky, M. de Koning, and T. D. de la Rubia, Philos. Mag. A **81**(5), 1257 (2001).
[29] J. Godet, L. Pizzagalli, S. Brochard, and P. Beauchamp, Comput. Mater. Sci. **30**(1–2), 16 (2004).
[30] S. Goedecker, T. Deutsch, and L. Billard, Phys. Rev. Lett. **88**(23), 235501 (2002).
[31] M. Heggie and R. Jones, Philos. Mag. B **48**(4), 365 (1983).
[32] A. Valladares and A. P. Sutton, J. Phys.: Condens. Matter **18**, 3735 (2006).
[33] A. Moulin, M. Condat, and L. P. Kubin, Philos. Mag. A **79**(8), 1995 (1999).
[34] M. D. Uchic, D. M. Dimiduk, J. N. Florando, and W. D. Nix, Science **305**, 986 (2004).
[35] T. Kizuka, Y. Takatani, K. Asaka, and R. Yoshizaki, Phys. Rev. B **72**, 035333 (2005).
[36] K. C. Lu, W. W. Wu, H. W. Wu, C. M. Tanner, J. P. Chang, L. J. Chen, and K. N. Tu, Nano Lett. **7**(8), 2389 (2007).
[37] A. S. B. S. G. Roberts and P. B. Hirsch, Mater. Sci. Eng. A **176**, 91 (1994).
[38] J. Rabier, P. Cordier, J. L. Demenet, and H. Garem, Mater. Sci. Eng. A **309–310**, 74 (2001).

 © 2009 WILEY-VCH Verlag GmbH & Co. KGaA, Weinheim